Materialia 11 (2020) 100740

Contents lists available at ScienceDirect

Materialia

journal homepage: www.elsevier.com/locate/mtla

Full Length Article

Friction stir butt welding of a high strength Al-7050 alloy with a metastable transformative high entropy alloy

S.S. Nene, S. Gupta, C. Morphew, R.S. Mishra*

Center for Friction Stir Processing, Department of Materials Science and Engineering, University of North Texas, Denton, Texas 76207, USA

ARTICLE INFO

Keywords:
Metastable high entropy alloy
Dissimilar metal joining
Aluminum alloy
Friction stir welding
Joint strength

ABSTRACT

A metastable transformative $Fe_{39}Mn_{20}Co_{20}Cr_{15}Si_5Al_1$ high entropy alloy (Al-HEA) was friction stir butt welded with Al-7050 alloy. Extensive mechanical mixing was evident in the weld nugget wherein sheared HEA particles were dispersed in Al-alloy matrix. Detail investigation of the weld interface showed suppression of intermetallic formation thereby approaching a clean interface. Tensile testing of the weld nugget showed a strength of 400 MPa with ~ 10% ductility whereas corrosion testing showed no sign of extensive pitting at the Al-HEA/Al-7050 weld interface. Therefore, use of high entropy alloy is an effective pathway for obtaining strong dissimilar joints with high strength Al alloys for lightweight applications.

1. Introduction

Welding of two distinctly different materials like steel/Al alloys, Al/Mg alloys and steel/ Mg alloys is desirable in manufacturing industry for weight reduction and cost optimization [1-3]. Various attempts have been made to successfully join high strength Al alloys with steel by using conventional fusion welding routes or high power density methods such as laser or electron beam welding. Maintaining the planar interface during solidification and avoiding liquation cracking in weld pool has been a tough challenge during welding of most of the Al alloys with Fe rich alloys such as steels [1-3]. The thermodynamically favorable phase separation causes excessive segregation and partial melting which deteriorates the overall weld properties during fusion welding [1-3]. Thus, solid state welding provides potential solution due to elimination of melting of the weld metals [3,4]. However, though melting was avoided, the extensive modulus mismatch between steel and Al alloys resulted in inferior solid state welded joints between these material under loading [3-5]. A survey of the literature on dissimilar Al alloy welding with steels shows that a number of attempts have been made to join 2XXX, 5XXX and 6XXX series Al alloys with steels for lightweight applications. However, high strength 7XXX series were observed to be less weldable with steels, limiting high strength applications.

Among all solid state welding techniques, friction stir welding (FSW) is used as primary welding route due to synergistic action of heat as well as plastic deformation [3,4]. Even though FSW has a reduced thermal cycle, issues like formation of intermetallic (IMC) layer due to reactivity between parent materials still remain topic of research [4-6]. It has been observed that though the thickness of IMCs formed during FSW is much lower than conventional fusion welds, the IMC layer remains weakest region in the weld promoting weld de-bonding. Thus, the weld strength is controlled by engineering the IMC formation which decides the fracture path under load. This remains a very crucial step towards improving joint efficiency [4-6].

Previous attempts were made to tune the IMC formation in variety of dissimilar weld combinations by trying to perform welding by either solid state or hybrid routes [1-6]. The present approach is towards engineering the IMC formation through modified alloy design technique. Over the last decade, researchers have explored a very exciting alloy design path based on high configurational entropy (ΔS_{conf}) [7]. According to this strategy, formation of intermetallic phases/compounds can be minimized by maximization of ΔS_{conf} of the alloy system at high temperature [8]. Increased ΔS_{conf} was achieved by moving away from the single principal element in the alloy to multiple principal elements leading to design of variety of high entropy alloys (HEAs) till date. However, the current understanding is that solute partitioning do take place in HEAs based on solidification path; however, liquid metal prefers to solidify in a disordered solid solution rather than IMCs. Hence, conceptualized that this approach can suppress IMC formation in welding. Substantial research efforts have been made to study weldability of different high entropy alloys by various welding methods. It has been seen that solid-state welding approach is more viable than fusion welding to maximize the welding efficiency and minimize the welding defects [9-14].

The present work used a newly designed metastable transformative high entropy alloy $Fe_{39}Mn_{20}Co_{20}Cr_{15}Si_5Al_1$ (all values in at.%) with 7XXX series Al alloy. The alloy design strategy for the $Fe_{39}Mn_{20}Co_{20}Cr_{15}Si_5Al_1$ (Al-HEA) was reported elsewhere [15-17].

* Corresponding author.
E-mail address: rajiv.mishra@unt.edu (R.S. Mishra).

https://doi.org/10.1016/j.mtla.2020.100740
Received 7 April 2020; Accepted 9 May 2020
Available online 19 May 2020

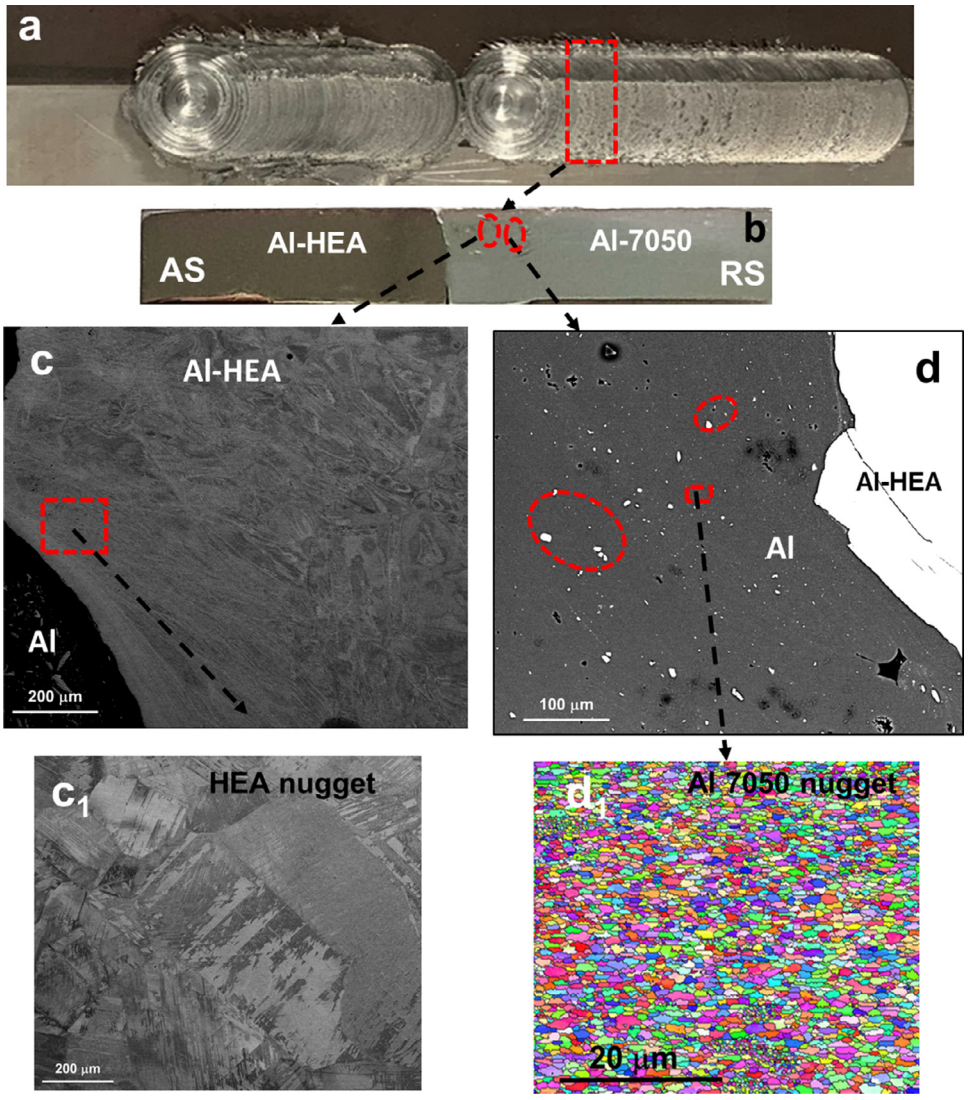

Fig. 1. Microstructural evolution along the Al-7050-T7 alloy/Al-HEA weld cross-section: (a) photographic image of the clean FSW runs showing no surface defects, (b) photographic image of weld cross-section showing the FSW nugget, (c) Low magnification back scattered imaging of Al-HEA side of the FSW nugget, (c_1) high magnification back scattered imaging of Al-HEA side of the FSW nugget, (d) low magnification back scattered image of Al-7050 T7 side of the FSW nugget, and (d_1) high magnification back scattered image of Al-7050 T7 side of the FSW nugget.

FSW of conventional steel with an Al 7050 alloy had formation of Fe-Al IMCs which act as a stress raiser leading to weld de-bonding [5,6]. This work not only reports successful joining of a high strength 7XXX alloy with a high strength steel like HEA but also proposes a new strategy to minimize the IMC formation at the weld interface.

2. Experimental Methods

$Fe_{39}Mn_{20}Co_{20}Cr_{15}Si_5Al_1$ plate was fabricated by casting in a vacuum induction melting furnace with nominal composition and subsequent rolling at 900°C, to achieve 50% reduction. The plate was then homogenized at 1200°C for 1 hr followed by water quenching. A rectangular piece of 160 × 75 × 6.5 mm^3 was cut from the rolled plate and friction stir welded with Al-7050 alloy plate having similar dimensions. A W-Re tool with a shoulder diameter of 16 mm, root diameter of 7.5 mm, pin diameter and length of 5 mm and 3.9 mm, respectively, was used for FSW. FSW was carried out with the parameters listed in Table 1. A Cu backing plate was used for effective heat dissipation, and Ar was blown near the workpiece/tool interface to avoid oxygen pickup during processing.

Metallographic specimens of weld cross section were prepared starting from 600 grade emery paper polishing followed by final polishing with 0.02 μm colloidal silica. Microstructures for all these conditions were analyzed by FEI NOVA Nano-SEM having electron backscatter diffraction (EBSD) and EDAX attachments and the data were analyzed using TSL OIM 8 software. X-ray diffraction (XRD) measurements were performed using a RIGAKU X-ray equipment equipped with Cu K_α radiation operated at 40 kV and 30 mA. Rectangular 1 mm-thick, dog-bone-shaped mini-tensile specimens were machined from welding nugget perpendicular to the butt welding bead using a computer numerical control (CNC) machine from 1 mm below the surface. Gage length and width of the tensile specimens were 5 and 1.25 mm, respectively. Electro-chemical studies of the weld were conducted in 3.5 wt.% NaCl solution at least three times to confirm repeatability of results. Potentiodynamic polarization scans were made with scan rate of 0.166 mV/s. All electrochemical measurements used saturated calomel electrode (SCE) as reference electrode and platinum as counter electrode.

Table 1
Processing parameters for FSP.

Processing parameters	S350
Rotational Rate (RPM)	350
Traverse Speed (mm/min)	50.8
Plunge Depth (mm)	4.1
Tilt Angle (°)	-2.5

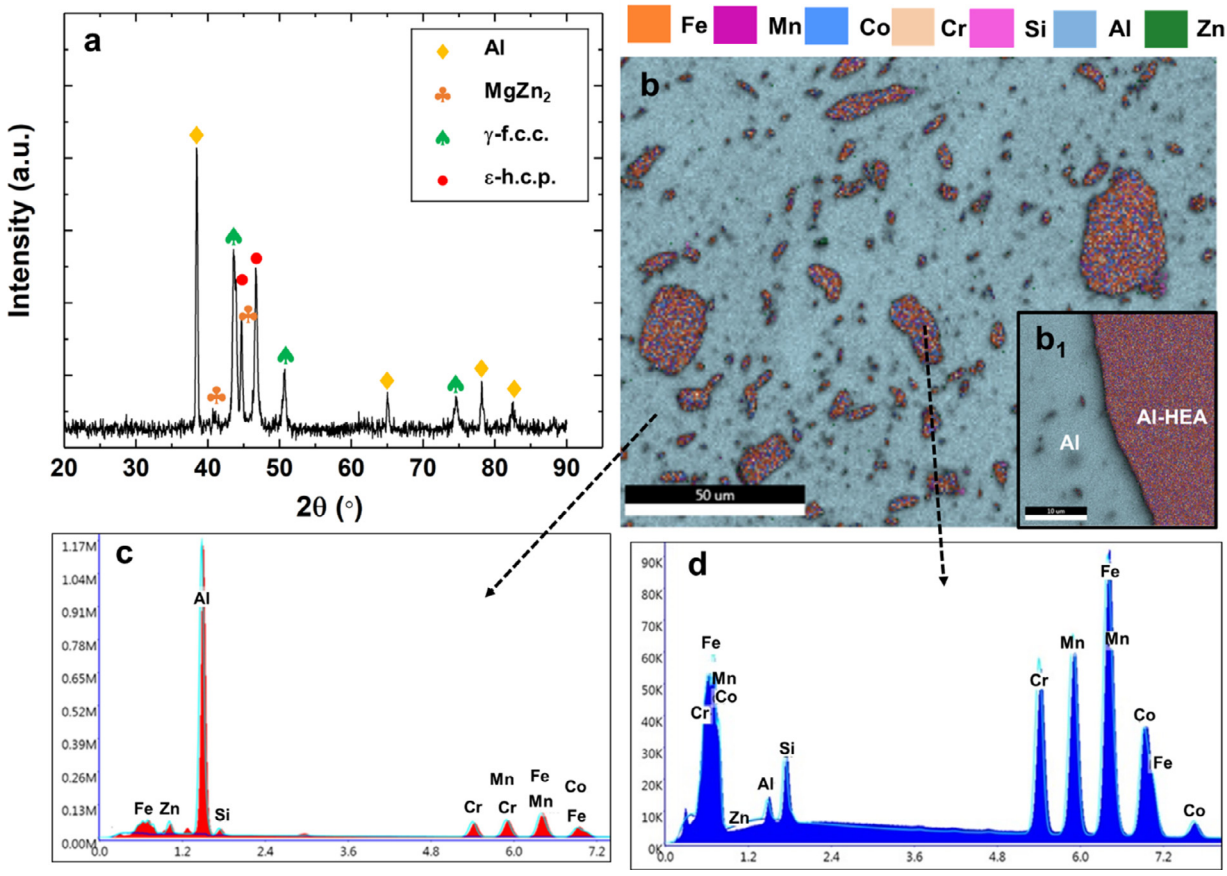

Fig. 2. Phase evolution in Al7050 T7 alloy/Al-HEA weld: (a) X-ray diffraction pattern indexed with the phases present in the weld nugget, (b) EDS X-ray mapping for the weld nugget showing dispersion of varying size Al-HEA particles, (b_1) EDS X-ray mapping of Al-7050 alloy/Al HEA interface at higher magnification showing cleaner interface, (c,d) EDS spectra for the Al-matrix and the Al-HEA dispersed in the weld nugget (EDS: Energy dispersive spectroscopy, HEA: high entropy alloy).

3. Results and Discussion

Figs. 1(a)–(d_1) summarize the microstructural evolution in the nugget along the cross section of the weld. Fig. 1(a) presents clear evidence of the welding beads being clean, and no evidence of any surface defects. Fig. 1(b) further confirms that there is no worm hole due to incomplete filling along the weld cross section, thereby suggesting sound welding of Al-HEA with Al-7050 alloy. As the welding was carried out with an offset such that only the upper portion of the pin should touch the Al-HEA, it barely got friction stirred, as seen in Fig. 1(c), which captures overall microstructure along the Al-HEA side (advancing side, AS). Thus, tool pin edge cuts the Al-HEA and displaces the broken particles along the run during the traverse of the tool. As a result, these broken particles mix with the plasticized Al matrix on the AS and get dispersed. Fig. 1(d) captures such dispersed Al-HEA particles in the Al- alloy matrix, as highlighted in red circles.

As the plunging was done in the Al-alloy, substantial plasticization assisted stirring is evident in the overall microstructure shown in Fig. 1(d) on Al alloy side (retreating side, RS). High magnification back scattered imaging (BSE) on RS side showed relatively coarser microstructure with formation of ε-martensite variants in the form of plates, although EBSD inverse pole figure (IPF) map for Al alloy in the nugget region (Fig. 1(d_1)) displayed extremely refined equiaxed microstructure. Along with the refined microstructure, sheared HEA particles are seen embedded in the Al matrix and form an in-situ composite type structure on the RS of the weld.

Figs. 2(a)–(d) capture the extensive mixing of Al-HEA and Al-alloy that occurred during FSW and resultant phase evolution in the weld nugget. As confirmed by the X-ray diffraction (XRD) pattern from the weld interface, there are pronounced peaks for Al and $MgZn_2$ which are the primary phases in the Al-7050 alloy. Along with these peaks, presence of γ and ε peaks is also evident from the XRD which suggest that the HEA particles embedded within the Al matrix have dual phase structure. There was no evidence of any extra peak in XRD pattern corresponding to the traditional Al-Fe intermetallic phases which hints that weld interface was cleaner and IMC formation was minimized. EDS X-ray mapping and area scanning of the interface region also showed dominance of Al on the Al side and Fe, Mn, Co, Cr, Si dominance in HEA particles suggesting very low reactivity among these materials at the weld interface [6-8,15-18].

Figs. 3 (a)-(d) display the overall mechanical response of the Al-HEA/Al-7050 weld from uniaxial tensile and hardness tests. As seen from the engineering stress-engineering stain curves, the weld has lower strength compared to both the base materials. However, similar uniform ductility was observed in comparison with Al-7050 alloy and work hardening rate (WHR) was comparable to Al-HEA. Fig. 3(a_1) show the mini-tensile specimen machined out of the weld region (perpendicular to the friction stir bead) which clearly depicts that the entire gage of the specimen was from the mixed region (nugget) of the Al-HEA/Al alloy weld. Thus, the tensile property shown in Fig. 3(a) is representative of the weld nugget. Hardness was also measured along the same region (Figs. 3(a, b) inset) from where the mini tensile specimens were machined (i.e. indents were made along the nugget region) to make the results comparable. Hardness distribution within the nugget appears scattered with an average value of 325 HV due to random distribution of the HEA particles embedded in the Al-matrix. The peak value of hardness obtained

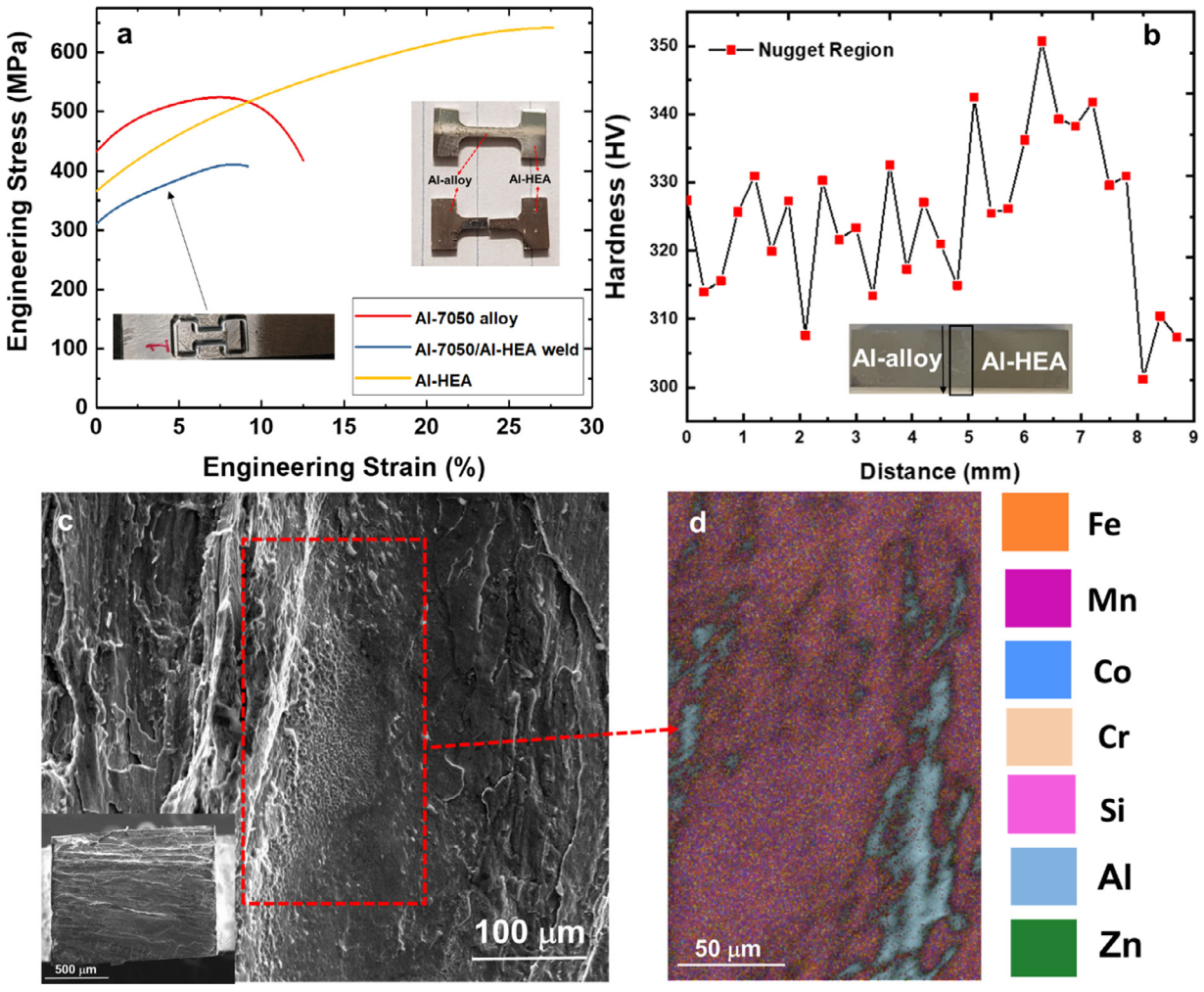

Fig. 3. Mechanical properties of the Al-7050T7/Al-HEA weld: (a) Engineering stress-engineering strain curves for weld nugget compared with the Al alloy and Al-HEA base materials, (b) hardness profile across the weld run, (c) secondary electron image of the fracture surface of the weld nugget after complete tensile deformation, and (d) EDS X-ray mapping of the highlighted region from the (c).

in the hardness distribution is associated with the indentation on the hard HEA particles present in the Al matrix. When compared with the Al alloy/304 stainless steel butt joint [19,20] (250 MPa, 300 HV [19]), the Al-7050/Al-HEA butt joint showed superior mechanical properties in terms of strength-ductility and hardness values after FSW.

Fig. 3(c) shows the secondary electron image of the fracture surface of the weld nugget specimen after complete tensile deformation. The fracture surface showed presence of both fine dimpled region as well as sheared regions indicating occurrence of a mixed mode failure. EDS-x-ray mapping of the fracture surface further revealed that, the fine dimpled region belonged to mainly HEA whereas shearing mainly occurred at Al-alloy matrix. The modulus mismatch between HEA and Al alloy is responsible for non-uniform strain accommodation among the two. This non-uniform strain accommodation at the weld interface give rise to stress concentration which leads to weld separation. Thus controlling the size of the Al-HEA particles can effectively engineer the load transfer among the HEA particles and Al alloy thereby making the joint stronger and tougher. Thus, tuning the critical size and distribution of sheared Al-HEA particles can be achieved through parametric optimization for further improvement in joint efficiency [4,21,22].

Figs. 4(a)–(d_2) display the corrosion behavior of the Al-alloy/Al-HEA weld nugget in 3.5wt% NaCl solution. Fig. 4(a) compares the potentiodynamic plots of the weld nugget with the Al-alloy base, Al-HEA base and Al-HEA in as-FSP condition. It is clear from these Tafel plots that, weld has similar E_{corr} value with respect to Al matrix whereas similar i_{corr} as that for the Al-HEA. Thus, initiation of the corrosion is governed by the Al matrix and rate of corrosion is governed by the galvanic Al-HEA/ Al alloy interface. It is well established that, corrosion kinetics is influenced by the presence of the second phase particles/precipitates or dispersoids size and distribution, wherein fine size and uniform distribution makes the corrosion process more uniform. As a result, size and distribution of sheared Al-HEA particles decide the corrosion kinetics [23].

As far as weld nugget is concerned, it displayed similar anodic kinetics as that of Al matrix as depicted by the parallel blue and red curves (highlighted by the black circle in Fig. 4(a)) in anodic regime suggesting mechanism of corrosion is decided by the Al-matrix. This is as per expectation since most of the exposed volume to the corrosive media is from Al alloy matrix. However, presence of Al-HEA dispersoids in the Al alloy played a crucial role in the corrosion localization (i.e. galvanic coupling) and thereby controlling the corrosion kinetics as shown by the conventional BSE imaging and EDS-x-ray mapping of the corroded surface (Figs. 4(b-d_2)). EDS-X-ray mapping further showed that, the dispersed Al-HEA particles are not attacked galvanically showing unreacted dispersoids (highlighted by the yellow circles in Fig. 4(d)) within the corrosion reaction product of Al matrix [23].

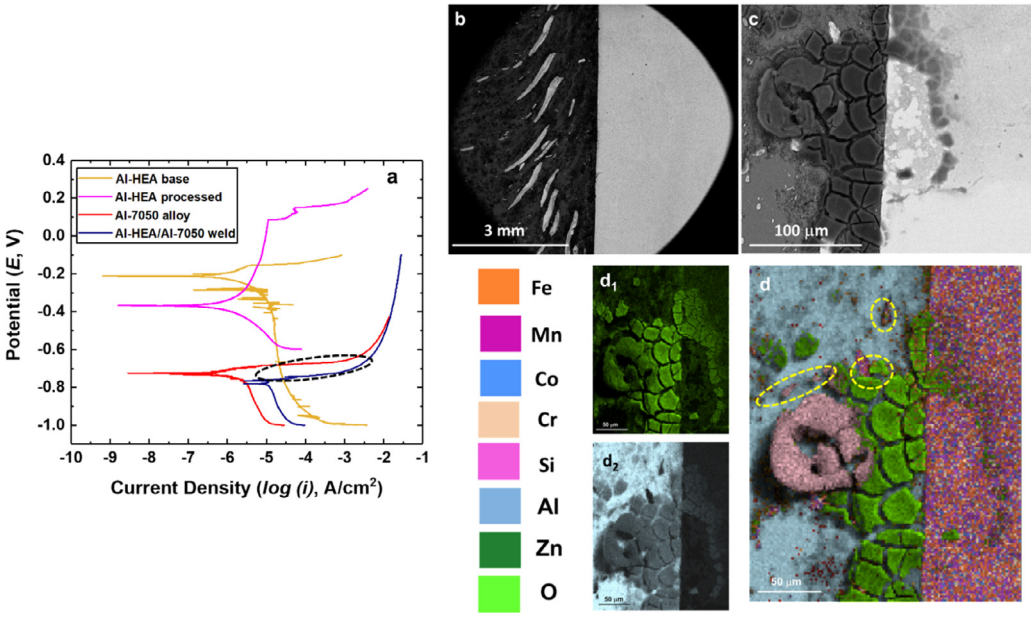

Fig. 4. Corrosion behavior of the Al-7050T7/Al-HEA weld: (a) potentiodynamic polarization plots for the weld nugget in comparison with the Al-HEA and Al alloy base materials, (b) low magnification back scattered electron image of the corroded volume of the weld nugget, (c) high magnification back scattered electron image of the corroded volume at the interface showing formation of corrosion product, (d) overlay image of the EDS X-ray scan taken on Fig. 4(c) showing the elemental distribution along the corroded volume, and (d_1 and d_2) EDS X-ray maps of the corrosion product showing dominance of Al and O in the corrosion product.

4. Conclusions

Friction stir welding of high strength Al-7050 T7 alloy with Al-HEA displayed defect free weld cross section with massive mechanical mixing of sheared HEA particles in the nugget. Primary results on the microstructural and phase evolution of the weld suggests no direct evidence of the intermetallic layer at the HEA/Al alloy interface suggesting sluggish reactivity during welding. Tensile testing resulted in ~80% joint efficiency with a strength and ductility values better than the stainless steel/Al alloy butt welds. Thus, the present work proposes a new pathway for obtaining strong butt joints of high strength Al alloys and Al-HEA with minimized IMC formation for lightweight applications.

Declaration of Competing Interest

The authors declare that they have no known competing financial interests or personal relationships that could have appeared to influence the work reported in this paper.

Acknowledgements

The work was carried out under the cooperative agreement of the University of North Texas with U.S. Army Research Laboratory (W911NF-18-2-0067). The authors thank Materials Research Facility (MRF) at University of North Texas for access to microscopy facilities.

References

[1] M. Pouranvari, S.P.H. Marashi, Critical review of automotive steels spot welding: process, structure and properties, Sci. Tech. Weld. Join. 18 (2013) 361.
[2] M.K. Kulekci, Magnesium and its alloys applications in automotive industry, Int. J. Adv. Manuf. Tech. 39 (2008) 851.
[3] W. Cai, G. Daehn, A. Vivek, H. Khan, R.S. Mishra, M. Komarasamy, A state-of-the-art review on solid-state metal joining, J. Manuf. Sci. Engg. 141 (2019) 031012.
[4] R.S. Mishra, Z.Y. Ma, Friction stir welding and processing, Mater. Sci. Engg., R 50 (2005) 1.
[5] T. Wang, H. Sridhar, R.S. Mishra, Y. Hovanski, P. Upadhyay, B. Carlson, Evaluation of intermetallic compound layer at aluminum/steel interface joined by friction stir scribe technology, Mater. Des. 174 (2019) 107795.
[6] T. Wang, M. Komarasamy, K. Liu, R.S. Mishra, Friction stir butt welding of strain-hardened aluminum alloy with highstrength steel, Mater. Sci. Engg., A 737 (2018) 85.
[7] J.W. Yeh, S.K. Chen, S. Lin, J.Y. Gan, T.S. Chin, T.T. Shun, C.H. Tsau, S.Y. Chang, Nanostructured high-entropy alloys with multiple principal elements: novel alloy design concepts and outcomes, Adv. Eng. Mater. 6 (2004) 299.
[8] D.B. Miracle, O.N. Senkov, A critical review of high entropy alloys and related concepts, Acta Mater 122 (2017) 448.
[9] Z. Wu, S.A. David, Z. Feng, H. Bei, Weldability of a high entropy CrMnFeCoNi alloy, Scripta Mater 124 (2016) 81.
[10] N. Kashaev, V. Ventzke, N. Stepanov, D. Shaysultanov, V. Sanin, S. Zherebtsov, Laser beam welding of a CoCrFeNiMn-type high entropy alloy produced by self-propagating high-temperature synthesis, Intermetallics 96 (2018) 63.
[11] Z.G. Zhu, Y.F. Sun, M.H. Goh, F.L. Ng, Q.B. Nguyen, H. Fujii, S.M.L. Nai, J. Wei, C.H. Shek, Friction stir welding of a $CoCrFeNiAl_{0.3}$ high entropy alloy, Mater. Let. 205 (2017) 142.
[12] Z.G. Zhua, Y.F. Sun, F.L. Ng, M.H. Goha, P.K. Liaw, H. Fujii, Q.B. Nguyen, Y. Xu, C.H. Shek, S.M.L. Naia, J. Wei, Friction-stir welding of a ductile high entropy alloy: microstructural evolution and weld strength, Mater. Sci. Eng., A 711 (2018) 524.
[13] D. Shaysultanov, N. Stepanov, S. Malopheyev, I. Vysotskiy, V. Sanin, S. Mironov, R. Kaibyshev, G. Salishchev, S. Zherebtsov, Friction stir welding of a carbon-doped CoCrFeNiMn high-entropy alloy, Mater. Charac. 145 (2018) 353.
[14] S. Park, C. Park, Y. Na, H. Kim, N. Kang, Effects of (W, Cr) carbide on grain refinement and mechanical properties for CoCrFeMnNi high entropy alloys, J. Alloys Compd 770 (2019) 222.
[15] S.S. Nene, K. Liu, M. Frank, R.S. Mishra, B.A. McWilliams, K.C. Cho, Extremely high strength and work hardening ability in a metastable high entropy alloy, Sci. Rep. 8 (2018) 9920.
[16] S.S. Nene, S. Sinha, M. Frank, K. Liu, R.S. Mishra, B.A. McWilliams, K.C. Cho, Unexpected strength–ductility response in an annealed, metastable,high-entropy alloy, App. Mater. Today 13 (2018) 198.
[17] S.S. Nene, M. Frank, K. Liu, S. Sinha, R.S. Mishra, B.A. McWilliams, K.C. Cho, Reversed strength-ductility relationship in microstructurally flexible high entropy alloy, Scripta Mater 154 (2018) 163.
[18] T. Wang, R.S. Mishra, Friction Stir Welding and Processing X, 2019, p. 33.
[19] M. Ghosh, R.K. Gupta, M.M. Husian, Friction Stir Welding of Stainless Steel to Al Alloy: Effect of Thermal Condition on Weld Nugget Microstructure, Met. Mater. Trans. A 45 (2014) 854.
[20] R. Sokkalingam, V. Muthupandi, K. Sivaprasad, K.G. Prashanth, Dissimilar welding of Al0.1CoCrFeNi high-entropy alloy and AISI304 stainless steel, J. Mater. Res. 34 (2019) 2683–2694.
[21] T. Wang, S. Shukla, S.S. Nene, M. Frank, R.W. Wheeler, R.S. Mishra, Towards Obtaining Sound Butt Joint Between Metallurgically Immiscible Pure Cu and Stainless Steel Through Friction Stir Welding, Met. Mater. Trans., A 49 (2018) 2578.
[22] P. Sahlot, S.S. Nene, M. Frank, R.S. Mishra, A. Arora, Towards attaining dissimilar lap joint of CuCrZr alloy and 316L stainless steel using friction stir welding, Sci. Tech. Weld. Join. 23 (2018) 715.
[23] S.S. Nene, M. Frank, K. Liu, S. Sinha, R.S. Mishra, B.A. McWilliams, K.C. Cho, Corrosion-resistant high entropy alloy with high strength and ductility, Scripta Mater 166 (2018) 168.